

# Multi-dimensional wind vibration coefficients under suction for ultra-large cooling towers considering ventilation rates of louvers

S.T. Ke<sup>\*1,2</sup>, L.Y. Du<sup>1a</sup>, Y.J. Ge<sup>2b</sup> and Y. Tamura<sup>3c</sup>

<sup>1</sup>Department of Civil Engineering, Nanjing University of Aeronautics and Astronautics, 29 Yuda Road, Nanjing 210016, China

<sup>2</sup>State Key Laboratory for Disaster Reduction in Civil Engineering, Tongji University, 1239 Siping Road, Shanghai 200092, China

<sup>3</sup>Center of Wind Engineering Research, Tokyo Polytechnic University, 1583 Iiyama, Atsugi, Kanagawa 243-0297, Japan

(Received April 19, 2017, Revised October 22, 2017, Accepted February 7, 2018)

**Abstract.** Currently, the dynamic amplification effect of suction is described using the wind vibration coefficient (WVC) of external loads. In other words, it is proposed that the fluctuating characteristics of suction are equivalent to external loads. This is, however, not generally valid. Meanwhile, the effects of the ventilation rate of louver on suction and its WV are considered. To systematically analyze the effects of the ventilation rate of louver on the multi-dimensional WVC of ultra-large cooling towers under suctions, the 210 m ultra-large cooling tower under construction was studied. First, simultaneous rigid pressure measurement wind tunnel tests were executed to obtain the time history of fluctuating wind loads on the external surface and the internal surface of the cooling tower at different ventilation rates (0%, 15%, 30%, and 100%). Based on that, the average values and distributions of fluctuating wind pressures on external and internal surfaces were obtained and compared with each other; a tower/pillar/circular foundation integrated simulation model was developed using the finite element method and complete transient time domain dynamics of external loads and four different suctions of this cooling tower were calculated. Moreover, 1D, 2D, and 3D distributions of WVCs under external loads and suctions at different ventilation rates were obtained and compared with each other. The WVCs of the cooling tower corresponding to four typical response targets (i.e., radial displacement, meridional force, Von Mises stress, and circumferential bending moment) were discussed. Value determination and 2D evaluation of the WVCs of external loads and suctions of this large cooling tower at different ventilation rates were proposed. This study provides references to precise prediction and value determination of WVC of ultra-large cooling towers.

**Keywords:** ultra-large cooling tower; wind tunnel test; ventilation rate; suction; external load; wind vibration coefficient

## 1. Introduction

As ultra-large cooling towers are typical wind sensitive structures (Kang 2016, Karakas *et al.* 2016, Asadzadeh *et al.* 2014, Li and Cao 2013), the wind vibration (WV) coefficient is a key parameter for design of ultra-large cooling towers. Current norms (GB50102-2014 2014, DL/T 5339-2006 2006, Sun and Zhou 1983, BS4485 1996, VGB-R610Ue 2005) and previous studies (Ke *et al.* 2015, Li and Li 2011, Zhou *et al.* 2014, Zhu *et al.* 2013) talking about determination of WVC focus on effects of external loads and propose that the WVCs under suctions are equivalent to those under external loads. In this case, the wind vibration effects induced by suctions are not precisely described and the effects of the ventilation rate of louver (see Fig. 1) on suction and its wind vibration are not considered. Therefore, it is of great significance to investigate the effects of the

ventilation rate of louver on the WVC of suction in the ultra-large cooling tower.

Ke *et al.* (2015) reported a study of value and distribution of WVC of an ultra-large nuclear tower using the consistent coupling method (Ke *et al.* 2015) and the results indicated that the WVC was maximized at the bottom and the throat leeside. In previous studies, time history of fluctuating wind was obtained using the AR method and the wind vibration response time domain of ultra-large cooling tower was calculated by combining the virtual excitation method (Li and Li 2011, Zhu *et al.* 2013). The results indicated that the displacement WVC of the tower was minimized in the middle part. Zhou *et al.* investigated the dynamic response characteristics of twin towers and cooling towers located in mountain area nearby and claimed that the WVC was increased in both cases (Zhou *et al.* 2014). Additionally, the effects of heights and configuration of ultra-large cooling tower on 3D distributions of its WVC were studied by involving aeroelastic measurement wind tunnel tests (Ke *et al.* 2013, Zhao *et al.* 2008, Babu *et al.* 2013, Ke and Ge 2014). This study provides references for the design of ultra-large cooling towers. Nevertheless, these studies focus on the WVC under external loads and the effects of suctions on the WVC were not considered. Also, the effects of ventilation rates of louver and response targets on the coefficient of suction-induced wind vibration were not considered, either.

\*Corresponding author, Associate professor  
E-mail: keshitang@163.com

<sup>a</sup>Postgraduate  
E-mail: dlynuaa@163.com

<sup>b</sup>Professor  
E-mail: yaojunge@tongji.edu.cn

<sup>c</sup>Professor  
E-mail: yukio@arch.t-kougei.ac.jp

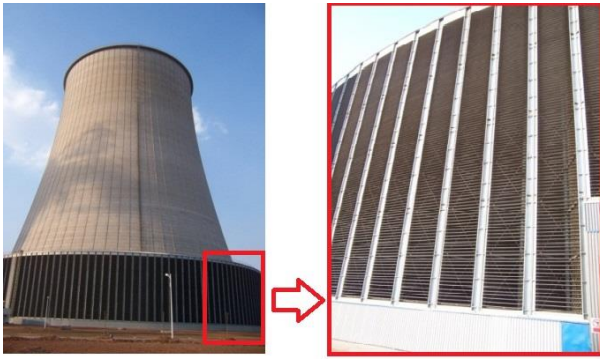


Fig. 1 Entire and local structure of louver in ultra-large indirect air cooling towers

Table 1 Main structural parameters of the ultra-large cooling tower

Structural parameter	Value (m)	Structural schematic
Tower top height	210	
Tower top radius	58	
Throat height	157.5	
Throat radius	55	
Inlet height	32.5	
Bottom diameter	90	
Wall thickness	0.37-2	
Pillar section	1.8×1.2	
Circular foundation section	12×2.5	

As a result, precise control of wind loads on ultra-large cooling tower and cost reduction have been limited.

Therefore, simultaneous rigid pressure measurement wind tunnel tests were executed on a 210 m ultra-large cooling tower under construction to obtain time history of fluctuating wind loads on the external surface and the internal surface of the cooling tower at different ventilation rates and curves of average wind pressures on external surface were compared with norms to verify the reliability of this approach. Based on that, the average values and distributions of fluctuating wind pressures on external and internal surfaces were obtained and compared with each other; a tower/pillar/circular foundation integrated simulation model was developed using the finite element method and complete transient time domain dynamics of external loads and four different suction of this cooling tower were calculated. Meanwhile, 1D, 2D, and 3D distributions of WVCs under four typical response targets (i.e., radial displacement, meridional force, Von Mises stress, and circumferential bending moment) were obtained and compared with each other. Finally, value determination and 2D evaluation of the WVCs of external loads and suction of this ultra-large cooling tower at different ventilation rates were proposed.

## 2. Background

An ultra-large indirect air cooling tower under

Table 2 Working conditions proposed in this study

Working condition	Description
Working condition 1	0% ventilation rate suction
Working condition 2	15% ventilation rate suction
Working condition 3	30% ventilation rate suction
Working condition 4	100% ventilation rate suction
Working condition 5	External load

construction in Northwestern China was studied in this case. This tower has a height of 210 m, bottom diameter of 180 m, throat height of 157.5 m, middle section radius of 55 m. The thickness of this tower is unified in different sections with maximum and minimum thickness of 2 m and 0.37 m, respectively. The tower bottom is attached to the circular foundation via 52 pairs of X-shaped pillars. Table 1 summarizes main structural parameters of the ultra-large cooling tower.

## 3. Wind tunnel tests

### 3.1 Working condition design

The additional ventilation rate of the air inlet (Referred to as ventilation rate) is the ventilation rate of the air cooling radiator which may exist in the inlet of the cooling tower, which is dependent on its construction stage and working conditions. In this study, three situations were proposed: (1) construction stage, 100% ventilation rate; (2) operation stage, 15% or 30% ventilation rate; (3) operation stage during winter, 0% ventilation rate. As the ventilation rate has negligible effects on external loads (Ke *et al.* 2015), the WVC of external loads was calculated by employing the time history of wind load corresponding to 30% ventilation rate of louver. Table 2 summarizes all working conditions proposed in this study.

### 3.2 Wind tunnel test design

The wind tunnel used is an atmosphere boundary layer, closed-loop one with a rectangular section of 5 m × 4 m. The rigid body model was in a scale of 1:400 and the internal surface for internal pressure tests were designed to be consistent. The blocking rate value in the wind tunnel test is 1.18%. For internal pressure tests, 200 measuring points were distributed uniformly along the meridian and the circumferential directions; for external pressure tests, 432 measuring points were distributed uniformly on the external surface. Fig. 2 shows the wind tunnel test models in five different working conditions and arrangement of measuring points in internal and external pressure tests. It should be noted that the analysis of wind tunnel test and finite element calculation conducted are based on the layout form with one single cooling tower.

The ground roughness element was placed in front of the inflow to facilitate wind fields simulations for atmosphere boundary layers in Category B landform. As shown in Fig. 3, the average and fluctuating wind speed

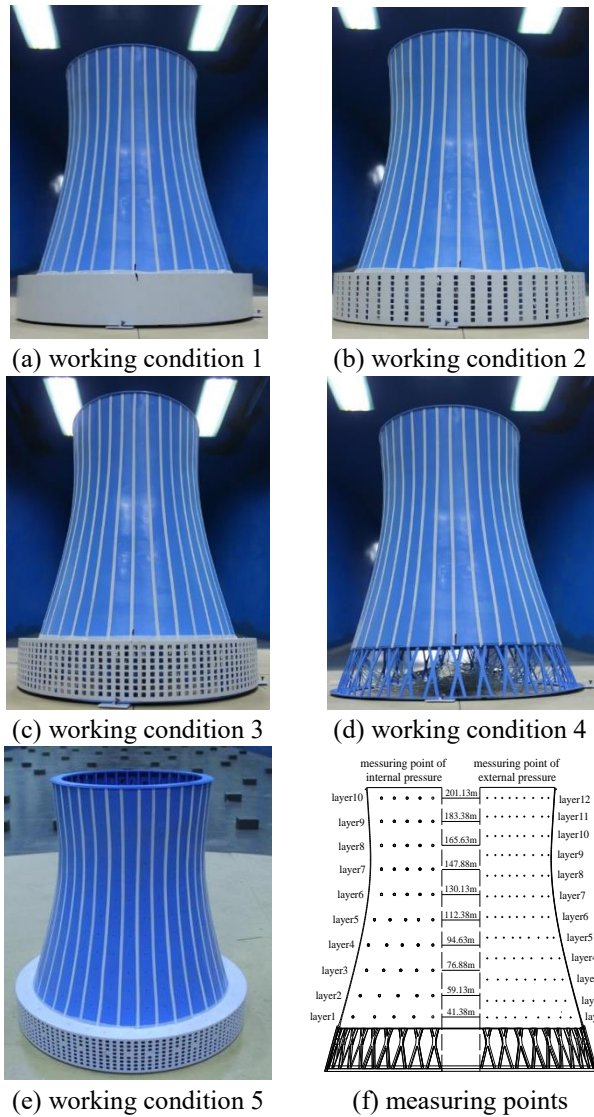


Fig. 2 Wind tunnel test models and the arrangement of measuring points

simulation was highly accurate. 36 vertical rough paper tapes (inter-tape distance = 5 mm) were arranged in two or three layers on the external surface to relieve Reynolds number incompatibility induced by scale reduction (Zhao *et al.* 2017, Cheng *et al.* 2016, Ke *et al.* 2015). Fig. 4 shows the external load coefficient of tower throat section and standard curves (GB50102-2014 2014, Sun and Zhou 1983, BS4485 1996, VGB-R610Ue 2005). As observed, the results obtained are highly consistent with national norm (GB50102-2014 2014), indicating excellent reliability.

### 3.3 Results and discussion

Fig. 5 shows average internal pressure coefficient curves of tower sections with meridional heights of 0-50 m, 50-100 m, 100-150 m, and 150-210 m as a function of the circumferential angle under diverse ventilation rates. The circumferential parameter is the angle and the radial parameter is the internal pressure coefficient. The following conclusions can be drawn:

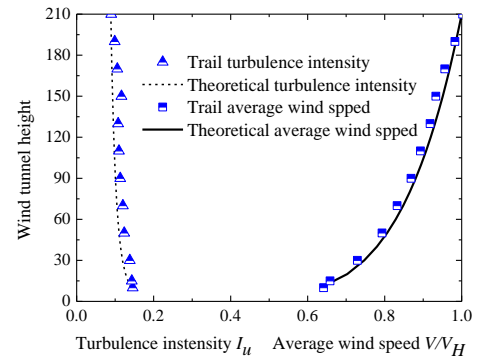


Fig. 3 Average wind speed and turbulence section

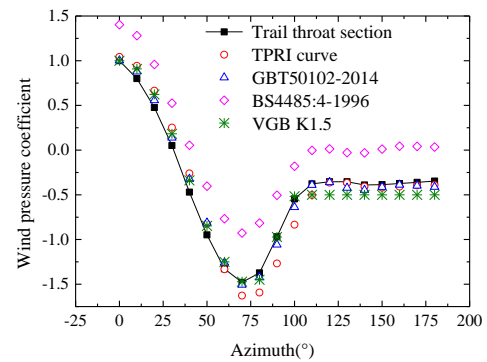


Fig. 4 Simulated external load coefficient curves considering the Reynolds number effect

a. In cases the ventilation rate is 0%, 15%, or 30%, the distributions of internal pressure coefficient are uniform and decreases as the circumferential angle increases.

b. In case the ventilation rate is 100%, the internal pressure coefficient fluctuates significantly, especially in the middle and lower parts. The minimized internal pressure coefficients of the middle and lower parts were -0.04 and -0.38, respectively, at angle of 144°. In the upper part, the minimized internal pressure coefficient (-0.40) was observed at angle of 144°.

c. The internal pressure coefficient in the upper part increased and then decreased as the ventilation rate increases. In cases the ventilation rate is 0%, the internal pressure coefficient fluctuates significantly with the circumferential angle and is minimized at angle of 144°. The internal pressure coefficient at the ventilation rates of 15% and 30% were maximized at angle of 324° to be -0.59 and -0.44, respectively.

Fig. 6 shows the mean square root curves of internal pressure coefficient of tower sections with meridional heights of 0-50 m, 50-100 m, 100-150 m, and 150-210 m as a function of the circumferential angle under different ventilation rates. As observed, the fluctuating amplitude of internal pressure coefficient follows the sequence of 0% > 15% > 100% > 30%. However, the mean square roots of the crosswind side and the leeward side internal pressure coefficients in 0-100 m and 150-210 m sections increased drastically (up to 0.25, at angle of 144°) at ventilation rate of 100%. The mean square root of internal pressure coefficient fluctuates significantly on the upper part of the tower.

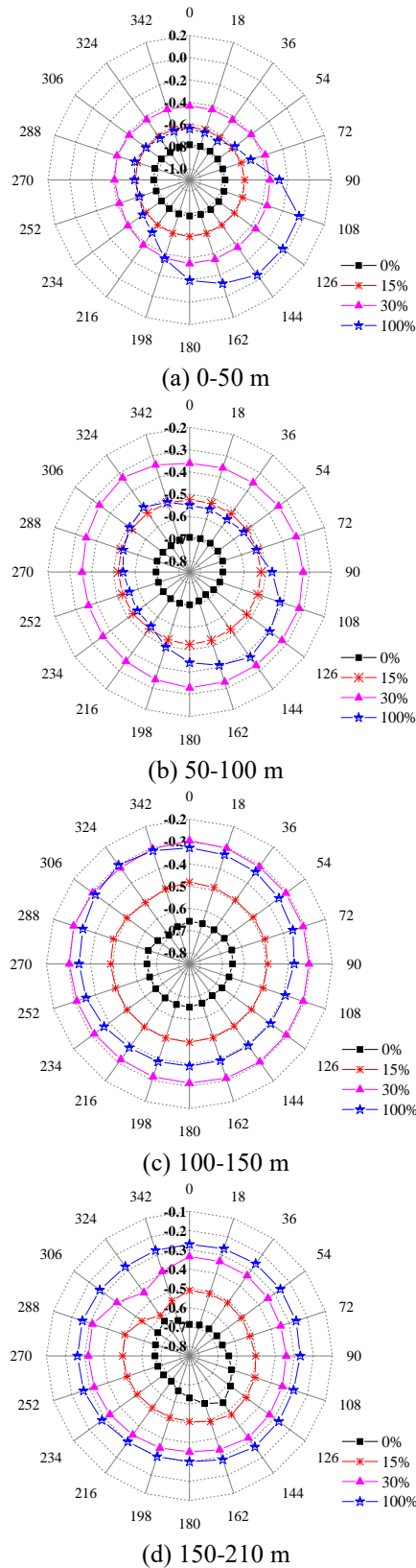


Fig. 5 Average internal pressure coefficients in typical tower sections at different ventilation rates

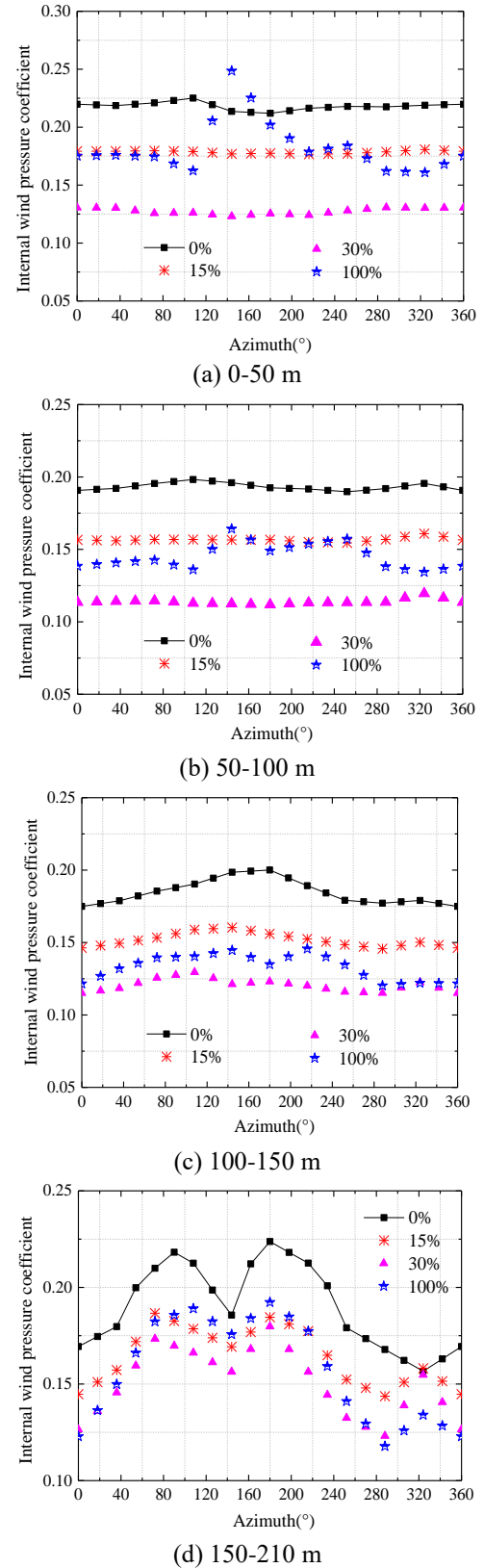


Fig. 6 MSR of internal pressure coefficients in typical tower sections at different ventilation rates

Fig. 7 shows the average and mean square root of external pressure coefficient of tower sections with meridional heights of 0-50 m, 50-100 m, 100-150 m, and

150-210 m as a function of the circumferential angle under different ventilation rates. As observed, the average external pressure coefficient curves on the windward side of the



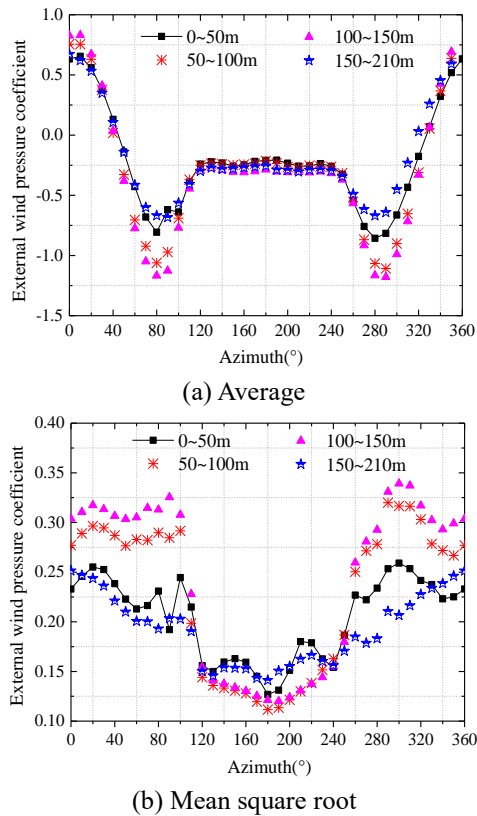


Fig. 7 Average and MSR of external pressure coefficient under different ventilation rates

tower sections are consistent. In the extreme negative pressure section, the average external pressure coefficient in 50-100 m and 150-210 m sections increased significantly and the average external pressure coefficient at the wind platform on the leeward side was relatively large. In 50-100 m and 150-210 m sections, the fluctuating amplitudes of external pressure coefficients along the circumferential angle were consistent. The average external pressure coefficient curves in 50-100 m and 100-150 m sections were highly consistent, the fluctuating amplitudes of external pressure coefficients on windward and leeward side varied significantly from values on the upper and lower parts of the tower and the maximum difference was 40.96%.

## 4. Finite element modeling and natural vibration analysis

### 4.1 Finite element modeling

Fig.8 shows the tower/pillar/circular foundation integrated simulation model established using ANSYS (Alam *et al.* 2012, Rahman and Alam 2015, Khan *et al.* 2016, Yeter *et al.* 2015, Qu *et al.* 2001). The tower, pillar/circular foundation, elastic foundation was represented using space shell units (SHELL63), beam units (BEAM188), and spring units (COMBINE14), respectively (a total of 29640 units). The circular foundation was attached to the tower and the pillar via multi-point

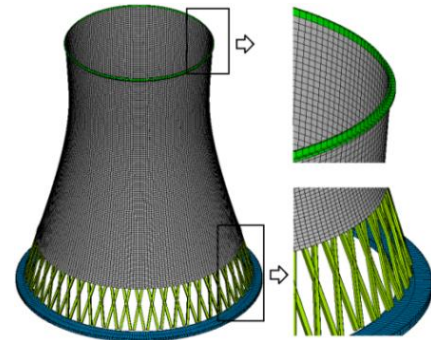


Fig. 8 Schematic of finite element model

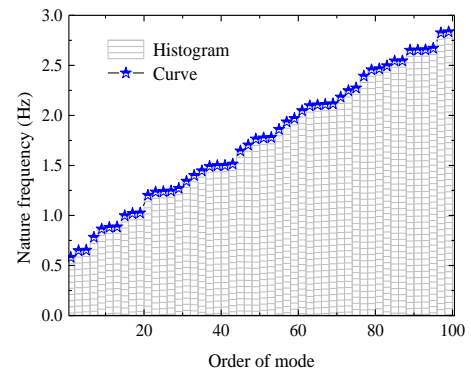


Fig. 9 First 100 order natural vibration frequency

constraining coupling and rigid domain, respectively. The bottom circular beam has a thickness of 2 m and the top has a rigid ring with thickness of 0.5 m and width of 1.1 m.

### 4.2 Characteristics of natural vibration

The dynamic characteristics were calculated using the Block Lanczos method (Berrabah *et al.* 2013), which is the default solver for ANSYS. This method is as accurate as the subspace method, but the solution is faster. Block Lanczos uses the coefficient matrix equation solver automatically, with which it is especially effective to extract the modal when calculating the natural frequency of a certain range included in the eigenvalue spectrum of a system.

Fig. 9 shows the first 100 order natural vibration curve and Table 3 shows the typical model parameters. As observed, the structural fundamental frequency of the ultra-large cooling tower is 0.58 Hz, which is lower than that of conventional cooling towers. The natural vibration shows a narrow distribution and increases linearly with the modal order.

Strong coupling between different models and varying vibration modes were observed, as well as random circumferential and vertical harmonic waves. The structure was overturned and the natural vibration frequency was maximized at the 30<sup>th</sup> order.

## 5. Calculation method and parameter

### 5.1 Calculation method

To solve transient dynamic equilibrium equations (Li *et*

al. 2013) of cooling towers, the core part is to describe transient states using the Newmark method (an implicit method) and the HHT method. Herein, the Newmark method involves finite difference method and in a time interval

$$[M]\{\ddot{u}\} + [C]\{\dot{u}\} + [K]\{u\} = \{F^a\} \quad (1)$$

$$\{\dot{u}_{n+1}\} = \{\dot{u}_n\} + [(1-\delta)\{\dot{u}_n\} + \delta\{\ddot{u}_{n+1}\}]\Delta t \quad (2)$$

$$\{u_{n+1}\} = \{u_n\} + \{\dot{u}_n\}\Delta t + [(\frac{1}{2}-\alpha)\{\ddot{u}_n\} + \alpha\{\ddot{u}_{n+1}\}]\Delta t^2 \quad (3)$$

Where  $\alpha$  and  $\delta$  are Newmark integration parameters.

Nevertheless, calculations of finite element discretion space domain using the Newmark method don't meet requirements of the algorithm, which states that solution precision degradation induced by numerical damping at high frequencies and generation of large quantity of numerical damping at low frequencies are not allowed. As a result, the HHT method was involved.

The HHT method is as follows

$$[M]\{\ddot{u}_{n+1-\alpha_m}\} + [C]\{\dot{u}_{n+1-\alpha_f}\} + [K]\{u_{n+1-\alpha_f}\} = \{F_{n+1-\alpha_f}^a\} \quad (4)$$

$$\text{Where } \{\ddot{u}_{n+1-\alpha_m}\} = (1-\alpha_m)\{\ddot{u}_{n+1}\} + \alpha_m\{\ddot{u}_n\};$$

$$\{\dot{u}_{n+1-\alpha_f}\} = (1-\alpha_f)\{\dot{u}_{n+1}\} + \alpha_f\{\dot{u}_n\};$$

$$\{u_{n+1-\alpha_f}\} = (1-\alpha_f)\{u_{n+1}\} + \alpha_f\{u_n\};$$

$$\{F_{n+1-\alpha_f}^a\} = (1-\alpha_f)\{F_{n+1}^a\} + \alpha_f\{F_n^a\}.$$

To maintain unconditional stability of the second-order system without sacrificing the accuracy of time integration,  $\alpha$ ,  $\delta$ ,  $\alpha_f$ , and  $\alpha_m$  should satisfy the following equation

$$\delta \geq \frac{1}{2}; \quad \alpha = \frac{1}{2}\delta; \quad \delta = \frac{1}{2} - \alpha_m - \alpha_f; \quad \alpha_m \leq \alpha_f \leq \frac{1}{2} \quad (5)$$

By combining Eqs. (2), (4), and (6), we can obtain

$$\begin{aligned} & (a_0[M] + a_1[C] + (1-\alpha_f)[K])\{u_{n+1}\} \\ & = (1-\alpha_f)\{F_{n+1}^a\} + \alpha_f\{F_n^a\} - \alpha_f\{F_n^{\text{int}}\} \\ & + [M](a_0\{u_n\} + a_2\{\dot{u}_n\} + a_3\{\ddot{u}_n\}) \\ & + [C](a_1\{u_n\} + a_4\{\dot{u}_n\} + a_5\{\ddot{u}_n\}) \end{aligned} \quad (6)$$

$$\text{Where } a_0 = \frac{1-\alpha_m}{\alpha\Delta t^2}, a_2 = \frac{1-\alpha_m}{\alpha\Delta t}, a_3 = \frac{1-\alpha_m}{2\alpha} - 1,$$

$$a_4 = \frac{(1-\alpha_f)\delta}{\alpha} - 1, a_5 = (1-\alpha_f)(\frac{\delta}{2\alpha} - 1)\Delta t.$$

In contrast Eqs. (4) and (6), it can be seen by I that the equilibrium equations of transient dynamics are realized by the linear combination of two successive steps in the HHT method.  $\alpha_m$  and  $\alpha_f$  are two additional parameters. The other two methods for determining parameters can also be used. When the amplitude attenuation factor  $\gamma$  is given, the other four parameters are

$$\alpha = \frac{1}{4}(1+\gamma)^2; \quad \delta = \frac{1}{2} + \gamma; \quad \alpha_f = 0; \quad \alpha_m = -\gamma \quad (7)$$

or

$$\alpha = \frac{1}{4}(1+\gamma)^2; \quad \delta = \frac{1}{2} + \gamma; \quad \alpha_f = \frac{1-\gamma}{2}; \quad \alpha_m = \frac{1-3\gamma}{2} \quad (8)$$

Table 3 Vibration modes of typical orders of cooling tower structure

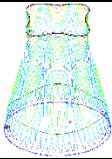
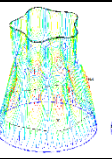


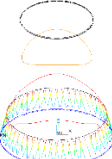
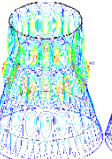
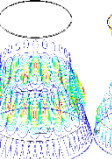

Order	1	5	10	20
Isopotential lines of vibration mode				
Frequency (Hz)	0.58	0.65	0.86	1.03
Harmonic number				
Circumferential	4	5	5	6
Vertical	1	2	2	3
Order	30	50	80	100
Isopotential lines of vibration mode				
Frequency (Hz)	1.27	1.77	2.47	2.84
Harmonic number				
Circumferential	1	9	12	4
Vertical	1	3	1	6

Table 4 Equivalent targets of WVC

Equivalent target	Radial displacement	Meridional force
Abbreviation	R-P	M-F
Equivalent target	Circumferential bending moment	Von Mises stress
Abbreviation	C-M	M-S

## 5.2 Parameters

The morphology of surrounding area was Category B morphology, the basic wind speed was 23.7 m/s, and the structural damping ratio was 5% (JGJ3-2010 2010). Table 4 summarizes WVCs at all measuring points based on four typical response targets. The equation is as follows

$$\beta_{Ri} = \frac{R_i}{\bar{R}_i} = 1 + \frac{g\sigma_i}{\bar{R}_i} \quad (9)$$

where  $\beta_{Ri}$  is the response WVC of the  $i$ th point,  $R_i$ ,  $\bar{R}_i$ , and  $\sigma_i$  are the overall response, average response, and fluctuating response of the  $i$ th point, and  $g$  is the peak value factor of the  $i$ th point, which is 3.0 in this case (Ke *et al.* 2012).

## 6. Comparison of WVCs

### 6.1 3D WVC

Figs. 10-14 show 3D distributions of WVCs coefficients corresponding to different equivalent targets under suction at different ventilation rates of louver. As observed, the circumferential and meridional WVCs of tower were significantly different. The WVCs coefficients calculated

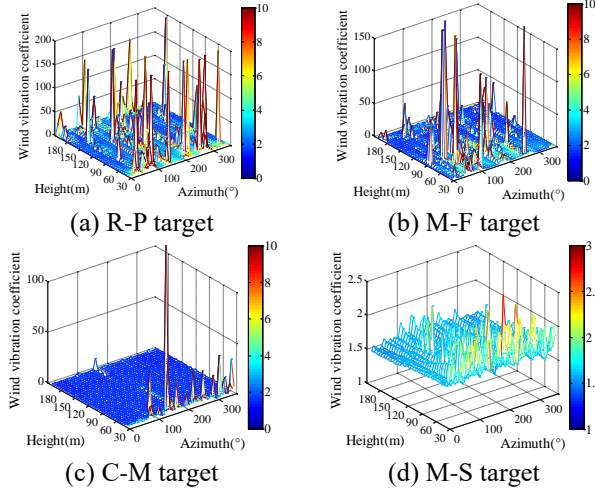


Fig. 10 3D distribution of WVC of louver under suction under working condition 1

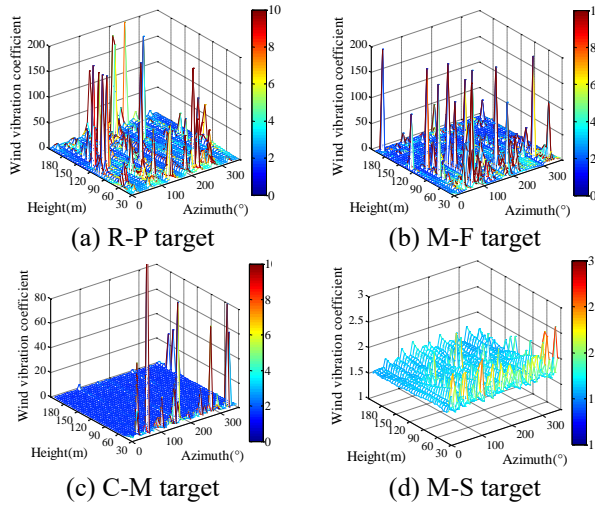


Fig. 11 3D distribution of WVC of louver under suction under working condition 2

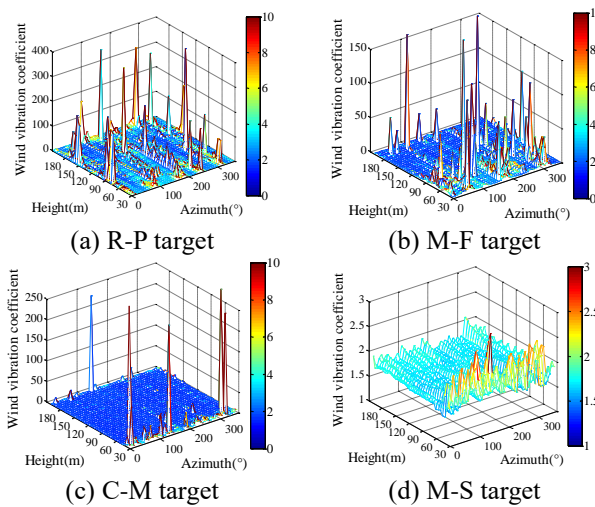


Fig. 12 3D distribution of WVC of louver under suction under working condition 3

using different equivalent targets varied significantly: the distortion of the value calculated using the R-P equivalent

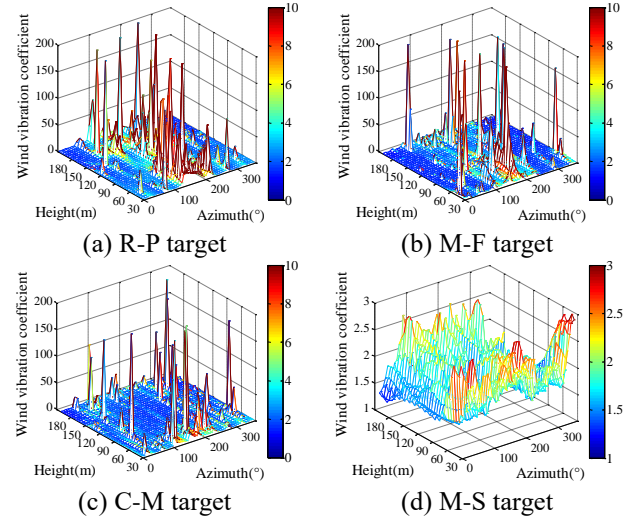


Fig. 13 3D distribution of WVC of louver under suction under working condition 4

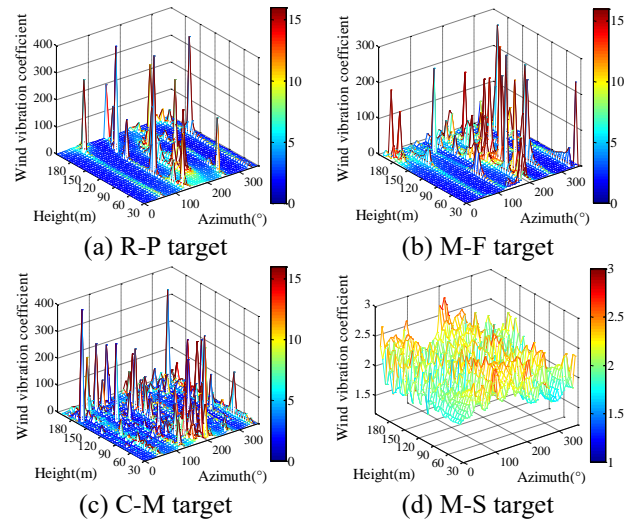


Fig. 14 3D distribution of WVC of louver under suction under working condition 5

target was maximized and the distortion of the value calculated using the M-S equivalent target was minimized. The distortion of WVC was usually observed on leeward side, bottom, and top of the tower, especially under working conditions 4 and 5.

## 6.2 2D meridional WVC

The meridional force and circumferential bending moment are the controlling factors for the structure design of cooling towers. Herein, the 2D WVC of the cooling tower structure was calculated with  $0^\circ$  meridian response as the equivalent target and the results are shown in Fig. 15. The following conclusions can be drawn:

a. The distributions of WVC coefficient with M-F and M-S equivalent targets were uniform compared with those with R-P and C-M equivalent targets. The WVC was minimized at ventilation rate of 100%.

b. The WVC under suction was large at the tower bottom and decreased as the height increased and then



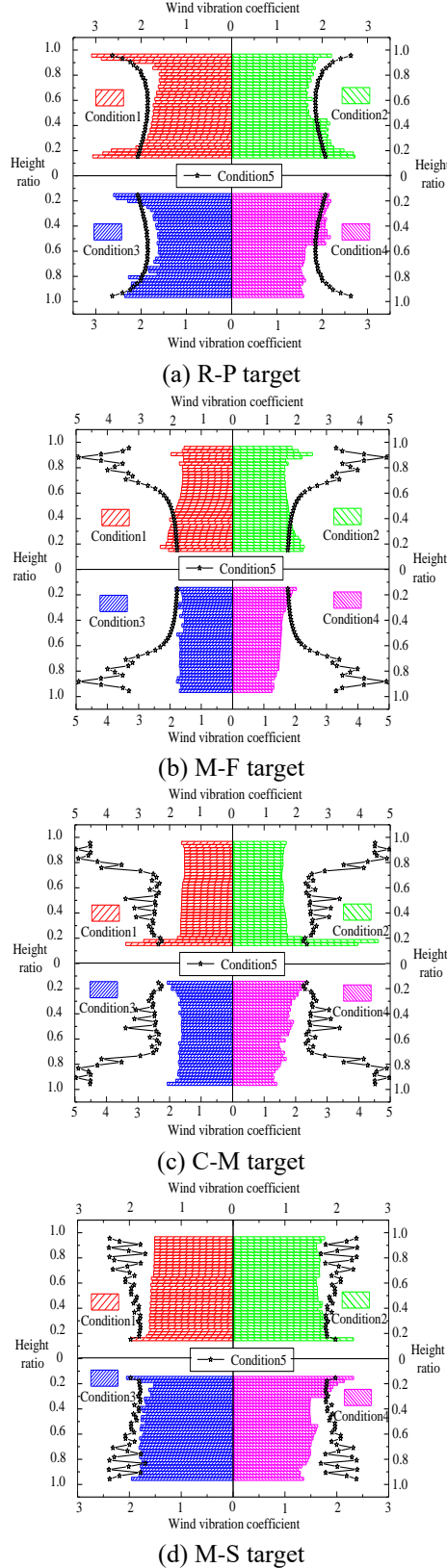


Fig. 15 2D meridional WVCs under suction and external loads with different equivalent targets and ventilation rates

increased once the height exceeds a critical level. The average and distributions of WVCs were dependent on the ventilate rate of louver.

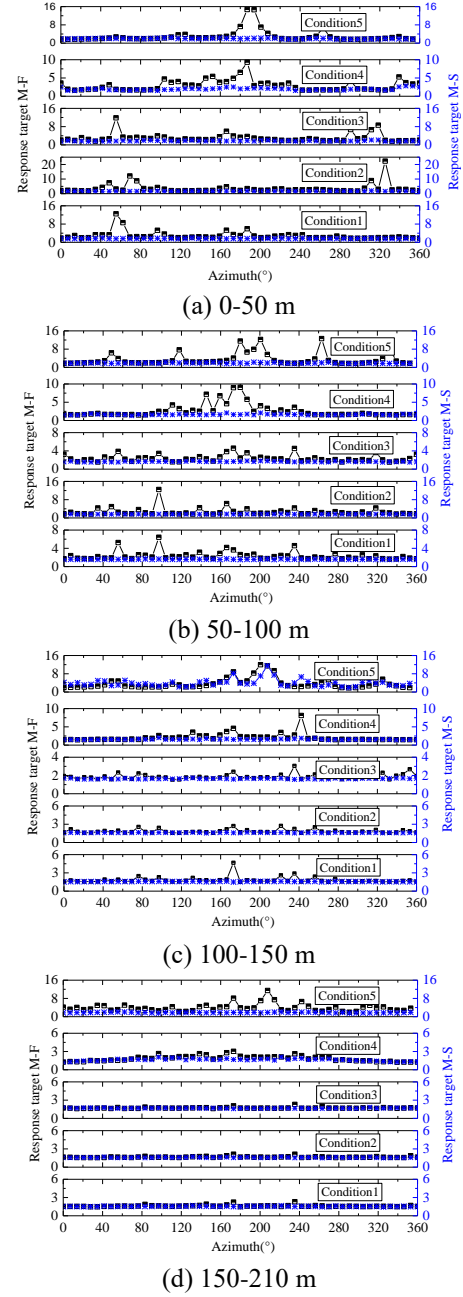


Fig. 16 Distributions of WVCs under suction and external loads on typical sections with M-F and M-S equivalent targets

c. The WVCs under external loads increased with the section height and fluctuated randomly in the upper part of the tower. At the tower bottom, the WVC under external loads was smaller than that under suction; in other sections, the WVC under external loads was larger than that under suction.

### 6.3 2D circumferential WVC

The 2D WVC as a function of the circumferential angle under different ventilation rates in tower sections with meridional heights of 0-50 m, 50-100 m, 100-150 m, and 150-210 m was investigated. The results indicated that the



Table 5 Recommended values of overall WVCs

Load	Ventilation rate	Equivalent target				Recommended value
		R-P	M-F	C-M	M-S	
Suction	0%	1.94	1.80	1.68	1.58	1.69
	15%	1.96	1.88	1.81	1.70	1.79
	30%	1.89	1.69	1.73	1.69	1.69
	100%	1.84	1.56	1.72	1.58	1.57
External load	30%	2.01	1.99	1.86	1.78	1.89

2D WVC with designated meridional force and uniformly distributed Von Mises stress as equivalent targets should be used for determination of the WVC of cooling tower structure. Fig. 16 shows distribution curves of circumferential WVCs with M-F and M-S response targets under different working conditions. The following conclusions can be drawn:

a. The uniformly distributed 2D circumferential WVCs under suctions were smaller than those under external loads.

b. Local peaks of the circumferential WVC under suctions with M-F response target were observed in all sections and the fluctuating amplitude of this parameter decreased as the tower height increased. Also, the frequency of local peaks of the circumferential WVC under suctions increased with the ventilation rate of louver.

c. The WVC was distributed uniformly along the circumferential angle in each section. At ventilation rate of 100%, the WVC increased, stayed constant, and then decreased along the circumferential angle in the 150-210 m section.

d. The WVC under external loads was consistent along the circumferential angle at M-S equivalent target, except in the 100-150 m section. Peaks of WVC under external loads were observed on the leeward side of the tower with M-F response target.

Fig. 17 shows the WVCs under suctions and external loads in different sections. These parameters were determined based on the distributions of 2D circumferential WVC with M-F and M-S equivalent targets. As observed, the WVCs under suctions increased with the section height and this parameter was maximized and minimized at ventilation rate of 15% and 100%, respectively. The wind vibration coefficients of cooling towers under different ventilation rates are quite different. Similarly, the WVCs under external loads increased with the section height.

#### 6.4 Overall WVC

The recommended values of WVCs under suctions at different ventilation rates of louver with different response targets were determined based on the study of 2D and 3D WVCs, as shown in Table 5. As observed, the WVCs under suctions were larger than those under external loads in all cases. The WVC under suctions was maximized at ventilation rate of 15%.

The average WVC with M-F and M-S equivalent targets were 1.69, 1.79, 1.69, and 1.57 at ventilation rates of 0%, 15%, 30%, and 100%, respectively, while the WVC under

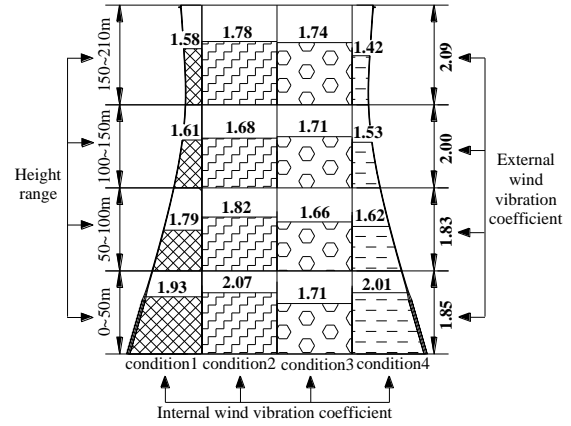


Fig. 17 Local distribution of WVCs in different sections

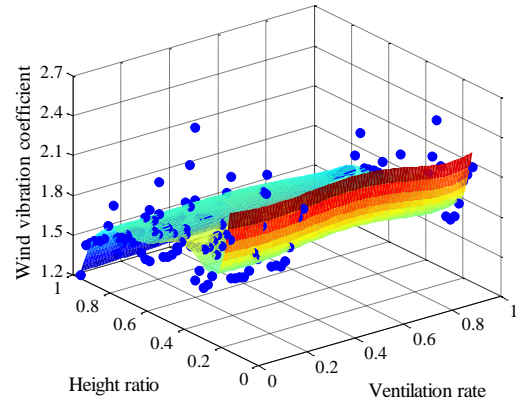


Fig. 18 Fitting surface of actual WVCs under sections with meridional force as response target

external loads were 1.89 and the standard WVC was 1.9. Therefore, it is recommended to employ WVC under suctions and external loads at corresponding ventilation rate of louver for structural design of cooling towers.

#### 6.5 Fitting equation of WVC

##### 6.5.1 Fitting equation of WVCs under suctions considering the ventilation rate of louver

As indicated by the results of this study, the WVCs ultra-large cooling towers of under suctions are directly related to the ventilation rate of louver and the meridional height, whose effects have not been considered in the conventional design. To facilitate structural design of ultra-large cooling towers, a fitting equation of WVCs with 0° meridional force as the response target was proposed based on nonlinear least square method. The ventilation rate of louver and meridional height were set as the variables.

$$\begin{aligned} \beta(\eta, h) = & (b_1 + b_2 \times h + b_3 \times h^2 + b_4 \times \eta \times h + b_5 \times \eta^3 \\ & + b_6 \times h^3 + b_7 \times \eta^4 + b_8 \times h^4 + b_9 \times \eta \times h^3 \\ & + b_{10} \times \eta^2 \times h^2 + b_{11} \times \eta^5 + b_{12} \times h^5) \\ & / (1 + b_{13} \times e^{(b_{14} \times \eta + b_{15} \times h)}) \end{aligned} \quad (10)$$

Where  $\eta$  is the damping ratio,  $h$  is the ratio of meridian height,  $b_i$  ( $i=1, 2, \dots, 15$ ) is the fitting coefficient, as shown in Table 6.

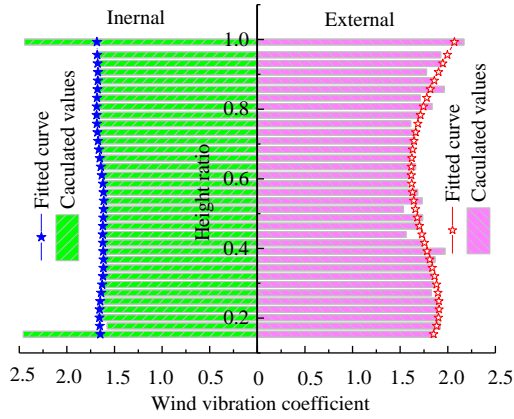


Fig. 19 Fitting curves of WVCs under suction and external loads at ventilate rate of 30%

Table 6 Coefficients in fitting equations of WVCs of cooling tower under suction considering the ventilation rate of louver

$i$	1	2	3	4	5	6	7	8
$b_i$	$1.31 \times 10^7$	$1.31 \times 10^8$	$-6.15 \times 10^8$	$-1.39 \times 10^6$	$-6.87 \times 10^6$	$1.29 \times 10^9$	$1.41 \times 10^7$	$-1.28 \times 10^9$
$i$	9	10	11	12	13	14	15	
$b_i$	$-5.62 \times 10^5$	$5.86 \times 10^5$	$-7.53 \times 10^6$	$4.81 \times 10^8$	$-1.16 \times 10^6$	0.17	1.90	

Table 7 Parameters for fitting equations of WVCs of cooling tower under suction and external loads at ventilation rate of 30%

Parameter	$i$	1	2	3	4	5
WVC under internal pressures	$a_i$	10.65	9.03	0.01	0.01	0.004
	$b_i$	2.24	2.47	14.56	22.49	32.74
	$c_i$	0.44	3.47	-2.25	-2.49	-6.40
WVC under external pressures	$a_i$	3.84	10.40	8.23	0	0
	$b_i$	2.60	4.92	5.16	0	0
	$c_i$	-0.40	1.10	4.06	0	0

Fig. 18 shows 2D distribution and fitting surface of WVCs of cooling towers with meridional force as response target as a function of ventilation rate of louver and meridional height. Herein, the blue points refer to the actual WVCs and the color surface indicates WVCs predicted by the fitting equation. As observed, at the bottom of the cooling tower, the wind-induced vibration coefficient is relatively large, but relatively small at the top. There are certain differences in the wind vibration coefficients of cooling towers under different ventilation rates.

### 6.5.2 Fitting equation of WVCs under suction and external loads at ventilation rate of 30%

The fitting equation for WVCs under suction and external loads at ventilation rate of 30% with meridional height as the variable is as follows

$$\begin{aligned} \beta(h) = & a_1 \times \sin(b_1 \times h + c_1) + a_2 \times \sin(b_2 \times h + c_2) \\ & + a_3 \times \sin(b_3 \times h + c_3) + a_4 \times \sin(b_4 \times h + c_4) \\ & + a_5 \times \sin(b_5 \times h + c_5) \end{aligned} \quad (11)$$

Where  $\beta(h)$  is the WVC,  $h$  is the ratio of meridional height,  $a_i$ ,  $b_i$ , and  $c_i$  are the fitting parameters summarized in Table 7.

Fig. 19 shows fitting curves of WVCs under suction and external loads at ventilate rate of 30%. As observed, fitting was effective in the middle part and throat of the tower, although the fitting effectiveness at the top and bottom of the tower was limited. Moreover, the WVCs under suction, which are distributed uniformly along the height, were smaller than those under external loads.

## 7. Conclusions

The 1D, 2D, and 3D distributions of WVCs of louver under suction at different ventilation rates were investigated and compared with those of external loads. Wind tunnel tests, finite element modeling, calculation of wind vibration responses, parameter analysis, and equation fitting were involved.

The results indicated that the ventilation rate of louver has a significant effect on the 3D distribution of WVC under suction and the fluctuating amplitudes were relatively small. The actual WVCs under suction corresponding to different working conditions can precisely reflect the wind vibration effect induced by suction in the cooling tower. The average (1.89) and fluctuating amplitude of WVCs under external loads were larger than those under suction. The WVCs at ventilation rates of 0%, 15%, 30%, and 100% were suggested to be 1.69, 1.79, 1.69, and 1.57.

Moreover, a two-dimensional evaluation equation for WVC under suction in ultra-large cooling towers as a function of ventilation rate of louver and tower height was proposed based on the nonlinear least square method. Also, a two-dimensional evaluation equation for WVC under external loads at ventilation rate of 30% was proposed. This study can provide references for accurate determination of WVCs under suction and external loads in ultra-large cooling towers.

## Acknowledgments

This project is jointly supported by National Natural Science Foundation (U1733129 and 51208254), Jiangsu Province Natural Science Foundation (BK2012390), Postdoctoral Science Foundation (2013M530255; 1202006B), Jiangsu Universities Qing Lan Project and Six Talent Peaks Project in Jiangsu Province (JZ-026), which are gratefully acknowledged.

## References

- Alam, M.N., Upadhyay, N.K. and Anas, M. (2012), "Efficient finite element model for dynamic analysis of laminated composite beam", *Struct. Eng. Mech.*, **42**(4), 471-488.
- Asadzadeh, E., Alam, M. and Asadzadeh, S. (2014), "Dynamic response of layered hyperbolic cooling tower considering the effects of support inclinations", *Struct. Eng. Mech.*, **50**(6), 797-816.
- Babu, G.R., Rajan, S.S., Harikrishna, P., Lakshmanan, N. and

- Arunachalam, S. (2013), "Experimental determination of wind-induced response on a model of natural draught cooling tower", *Exper. Tech.*, **37**(37), 35-46.
- Berrabah, H.M., Tounsi, A.L., Semmah, A. and Bedia, E.A.A. (2013), "Comparison of various refined nonlocal beam theories for bending, vibration and buckling analysis of nanobeams", *Struct. Eng. Mech.*, **48**(3), 351-365.
- BS 4485 (1996), *Code of Practice for Structural Design and Construction-Water Cooling Towers*.
- Cheng, X.X., Zhao, L. and Ge, Y.J. (2016), "Field measurements on flow past a circular cylinder in transcritical reynolds number regime", *Acta Phys. Sin.*, **65**(21).
- DL/T 5339-2006 (2006), *Code for Hydraulic Design of Fossil Fuel Power Plants*, The Ministry of Construction of China, Beijing, China.
- GB/T50102-2014 (2014), *Industrial Circulating Water Cooling Design Specification*, The Ministry of Construction of China, Beijing, China.
- JGJ3-2010 (2010), *Technical Specification for Concrete Structures of Tall Building*, The Ministry of Construction of China, Beijing, China.
- Kang, J.H. (2015), "Vibration analysis of free-fixed hyperbolic cooling tower shells", *Struct. Eng. Mech.*, **55**(4), 785-799.
- Karakas, A.I., Ozgan, K. and Daloglu, A.T. (2016), "A parametric study for free vibration analysis of hyperbolic cooling towers on elastic foundation using consistent fem-vlasov model", *Arch. Appl. Mech.*, **86**(5), 869-882.
- Ke, S.T. and Ge, Y.J. (2014), "The influence of self-excited forces on wind loads and wind effects for super-large cooling towers", *J. Wind Eng. Industr. Aerodyn.*, **132**, 125-135.
- Ke, S.T., Ge, Y.J. and Zhao, L. (2012), "A new methodology for analysis of equivalent static wind loads on super-large cooling towers", *J. Wind Eng. Industr. Aerodyn.*, **111**(3), 30-39.
- Ke, S.T., Ge, Y.J. and Zhao, L. (2015), "Wind-induced vibration characteristics and parametric analysis of large hyperbolic cooling towers with different feature sizes", *Struct. Eng. Mech.*, **54**(5), 891-908.
- Ke, S.T., Ge, Y.J., Zhao, L. and Tamura, Y. (2015), "Stability and reinforcement analysis of super large exhaust cooling towers based on a wind tunnel test", *J. Struct. Eng.*, **141**(12), 04015066.
- Ke, S.T., Liang, J., Zhao, L. and Ge, Y.J. (2015), "Influence of ventilation rate on the aerodynamic interference for two IDCTs by CFD", *Wind Struct.*, **20**(3), 449-468.
- Khan, A.A., Alam, M.N., Rahman, N. and Wajid, M. (2016), "Finite element modelling for static and free vibration response of functionally graded beam", *Lat. Am. J. Sol. Struct.*, **13**(4), 690-714.
- Li, G. and Cao, W.B. (2013), "Structural analysis and optimization of large cooling tower subjected to wind loads based on the iteration of pressure", *Struct. Eng. Mech.*, **46**(5), 735-753.
- Li, H.N., Tang, S.Y. and Yi, T.H. (2013), "Wind-rain-induced vibration test and analytical method of high-voltage transmission tower", *Struct. Eng. Mech.*, **48**(4), 144-150.
- Li, X. and Li, X.W. (2011), "Analysis of wind-induced dynamic response of super large cooling tower", *Build. Struct.*, **S1**, 1414-1417.
- Qu, W.L., Chen, Z.H., and Xu, Y.L. (2001), "Dynamic analysis of wind-excited truss tower with friction dampers", *Comput. Struct.*, **79**(32), 2817-2831.
- Rahman, N. and Alam, M.N. (2015), "Structural control of piezoelectric laminated beams under thermal load", *J. Therm. Stress.*, **38**(1), 69-95.
- Sun, T.F. and Zhou, L.M. (1983), "Without ribs the elliptic wind pressure distribution of the cooling tower full size measurement and wind tunnel study", *J. Air Dyn.*, **12**(4), 12-17.
- VGB-R 610Ue (2010), *Structural Design of Cooling Tower-Technical Guideline for the Structural Design, Computation and Execution of Cooling Towers*.
- Yeter, B., Garbatov, Y. and Soares, C.G. (2015), "Fatigue damage assessment of fixed offshore wind turbine tripod support structures", *Eng. Struct.*, **101**, 518-528.
- Zhao, L., Ge, Y.J. and Cao, F.C. (2008), "Equivalent beam-net design theory of aero-elastic model about hyperbolic thin-shell cooling towers and its experimental investigation", *J. Vibr. Eng.*, **21**(1), 31-37.
- Zhao, L., Ge, Y.J. and Kareem, A. (2017), "Fluctuating wind pressure distribution around full-scale cooling towers", *J. Wind Eng. Industr. Aerodyn.*, **165**, 34-45.
- Zhou, X., Niu, H.W., Chen, Z.Q. and Wang, Z.Y. (2014), "Study on interference effect of cooling towers under condition of tower-tower and hilly surroundings", *J. Build. Struct.*, **35**(12), 140-148.
- Zhu, J.N., Xu, Y.Z. and Li, X. (2013), "Stochastic wind-induced dynamic response analysis of large hyperbolic cooling tower", *J. Xi'an Univ. Architect. Technol.*, **45**(6), 808-812.

CC